Hot Spots in an Athermal System

Axelle Amon,[1] Van Bau Nguyen,[2] Ary Bruand,[3] Jérôme Crassous,[1] and Eric Clément[2]
[1]*Institut de Physique de Rennes (UMR UR1-CNRS 6251), Université de Rennes 1, Bâtiment 11A, Campus de Beaulieu, F-35042 Rennes, France*
[2]*PMMH, ESPCI, UMR CNRS 7636 and Université Paris 6 et Paris 7, 75005 Paris, France*
[3]*ISTO, UMR 6113, 45000 Orléans, France*
(Received 8 November 2011; published 28 March 2012)

We study experimentally the dynamical heterogeneities occurring at slow shear, in a model amorphous glassy material, i.e., a 3D granular packing. The deformation field is resolved spatially by using a diffusive wave spectroscopy technique. The heterogeneities show up as localized regions of strong deformations spanning a mesoscopic size of about 10 grains and called the ''hot spots.'' The spatial clustering of hot spots is linked to the subsequent emergence of shear bands. Quantitatively, their appearance is associated with the macroscopic plastic deformation, and their rate of occurrence gives a physical meaning to the concept of ''fluidity,'' recently used to describe the local and nonlocal rheology of soft glassy materials.

DOI: 10.1103/PhysRevLett.108.135502 PACS numbers: 81.40.Lm, 83.50.−v, 83.80.Fg

Amorphous glassy materials is a generic term representing many disordered systems where ''slow'' relaxations and complex dynamical processes take place under shear [1]. A remarkable feature is that the response to shear displays a phenomenology shared by many different materials quite independently of their microscopic physical or chemical details. They behave as solids at small applied stresses, and at higher applied stresses they undergo plastic deformation and then flow, with seemingly universal rheological laws [2–4]. Such generic behaviors are observed for concentrated emulsions [5], colloidal systems [6], foams [7,8], or molecular glasses [9]. Another striking observation is the emergence of complex spatiotemporal features such as cracks or shear bands [8,10–12] displaying complex avalanchelike statistics [13]. These observations have led to the proposition that only a limited number of ''universal'' scenarios may describe plasticity and the consequent rupture modes. The modern vision of plasticity in amorphous solids has brought to the front the concept of localized plastic events originally introduced by Argon [14]. Localized plastic events interact through long range elastic coupling and trigger irreversible macroscopic deformations. This vision extends naturally the notion of defect dynamics for crystalline solids. The activation, the dynamics, and the coupling of localized plastic structures are the object of numerous recent theoretical and numerical studies [9,15–19]. Coming from a different background, the theoretical description of the rheology of yield-stress fluids, often called the ''soft glassy rheology'' [2–4], is based on ideas of a similar flavor. This approach introduces an internal variable, often called ''fluidity,'' representing a rate of energy relaxation of internal processes and their spatiotemporal coupling. In several models, fluidity emerges as a macroscopic field which may couple nonlocally to the material rheology [20,21]. This description produces heterogeneities where fully developed flows and localized shear bands may coexist with quasijammed regions. The relation between fluidity and localized structures was suggested by Goyon *et al.* [5,22] in the theoretical analysis of an experiment of confined emulsions. Such an interpretation scheme was also used in a model experiment of sheared bubble rafts [23]. All these studies postulate the existence of discrete deformation events. Experimentally, localized plastic events may be identified as the foam $T1$ event [24] or directly observed in colloidal glasses by using confocal microscopy [25]. Visualization at the scale of the grain during a granular material friction experiment shows reorganizations prior to macroscopic sliding [26,27]. However, to our knowledge, the experimental link between the appearance of localized microscopic or mesoscopic events and the macroscopic plastic deformation is still missing as well as the role they might play in the path towards macroscopic material yield such as the formation of shear bands.

In this Letter, we address experimentally the relation between macroscopic mechanical properties and the occurrence of localized plastic deformations. To this purpose, we study a granular packing under shear as a model amorphous system, and we observe with a diffusive wave spectroscopy technique the deformation field at the surface. We show that the localized structures as conjectured by Argon [14] and observed in colloidal glasses do exist in such system. We observe that they are directly linked to the emergence of rupture into the material, and we link their rate of occurrence to plasticity and to the fluidity internal variable defined in rheological models.

Experimental method.—Our model amorphous material is an assembly of glass spheres (diameter $d = 200 \pm 30$ μm, packing fraction 0.60 ± 0.01) placed into an axisymmetric cylindrical of external radius $R = 5$ cm shear cell [Fig. 1(a)]. Shear is obtained by rotation of a four-blade vane (radius $R_0 = 1.27$ cm, height $H_0 = 2.54$ cm).

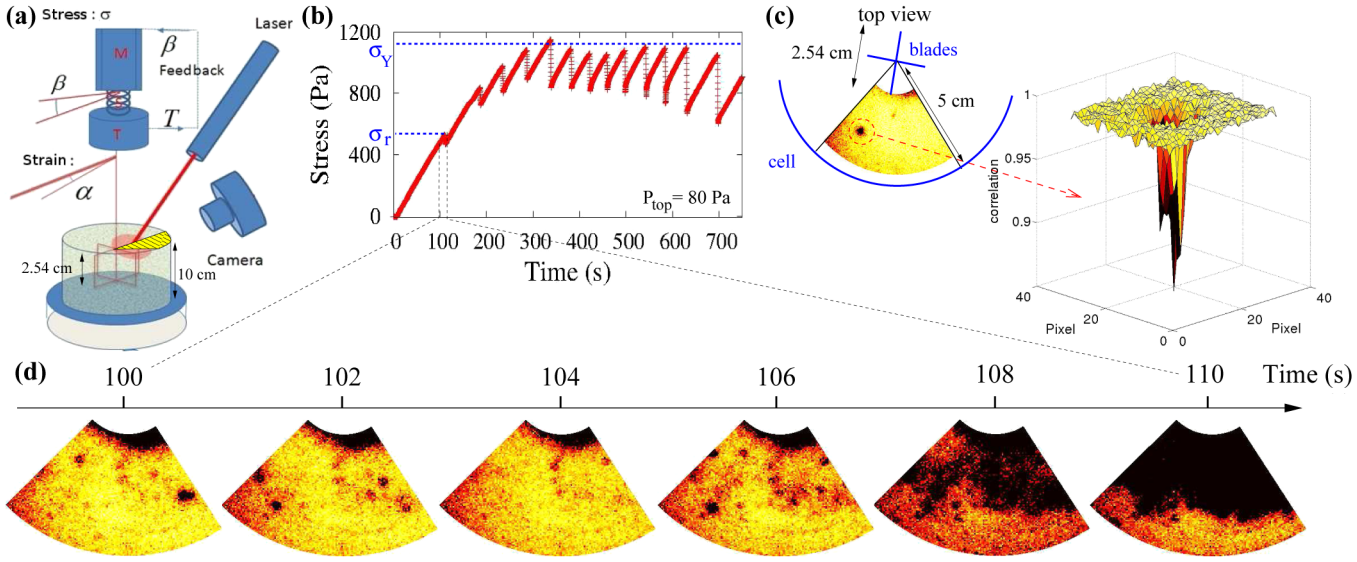

FIG. 1 (color online). (a) Schematic of the experimental setup. (M): motor, (S): torsion spring, (T): torque probe. A feedback loop allows us to impose the applied torque in creep experiments. A laser ($\lambda = 633$ nm) illuminates the top of the shear cell. The camera collects backscattered light. The surface of the sample is imaged on the camera sensor. (b) Stress response for an imposed deformation experiment (confining pressure $P_{\text{top}} = 80$ Pa, imposed rotation rate 7×10^{-3} rad $\cdot$ s^{-1}). (c) Part of the surface of the cell that is used for the correlation maps showing a typical localized spot: typically, in average $g_1 \simeq 0.99$ (yellow) and $g_1 \lesssim 0.95$ for the black spot. (d) Correlation maps between successive images corresponding to the first stress drop.

The filling height of the shear cell is $\simeq 10$ cm. The penetration depth of the vane is fixed so that the upper edge reaches the surface from below within a few grain sizes. During the insertion procedure, the material is gently fluidized by an air flux in order to obtain a controlled uniform compactness, deduced from *in situ* permeability measurement. The fluidization process is stopped during each mechanical measurement. The applied stresses and deformations are controlled by a step motor fixed to a torsional spring. The applied torque T and the rotation of the vane α are measured, giving access to the mean stress $\sigma = T/2\pi R_0^2 H_0$ and strain $\gamma = \alpha R_0/(R - R_0)$. The device is suited to work at an imposed motor rotation rate or at an imposed shear stress due to a feedback loop between the torque probe and the motor. Three different confining pressure conditions, P_{top}, have been tested: $P_{\text{top}} = 0$ corresponds to the free surface; for $P_{\text{top}} = 80$ Pa, a circular glass lid with a hole for the axis is placed on the glassy material; and for $P_{\text{top}} = 830$ Pa, supplementary loads are added on the glass lid. The phenomenology of the observations is not modified from one confining pressure to another. In addition to the mechanical measurements, we obtain a spatially resolved map of the surface deformations by using a diffusive wave spectroscopy (DWS) technique [28]. A laser illuminates the top of the shear cell. A camera imaging the surface at a frame rate of 1 Hz collects backscattered light. The correlation of scattered intensities between two successive images, g_1, is computed by zones of 16×16 pixels, composing correlation maps of 370 μm resolution [Fig. 1(c)]. For an homogeneous affine deformation ϵ, with $\epsilon_{ij} = (1/2)(\partial u_i/\partial x_j + \partial u_j/\partial x_i)$, where $\mathbf{u}$ is the displacement field, the variations of all the optical paths depend on the deformation tensor. It may be shown (see [29,30]) that, for diffusive waves, the path length variations are dependent on the combination of the stress tensor invariants $\bar{\epsilon} = \sqrt{(1/2) \times \text{Tr}^2(\epsilon) + \text{Tr}(\epsilon^2)}$. The variations of g_1 with $\bar{\epsilon}$ depend on the geometry of light illumination and detection. For a backscattering geometry, we obtain $g_1 \simeq \exp(-c\bar{\epsilon})$ with $c \simeq 2.5(2\pi l^*/\lambda)$, where l^* is the transport mean free path and λ is the optical wavelength. With $l^* \approx 3.3d$ for glass beads, we have $c \simeq 1.5 \times 10^4$. The average probed depth is $\simeq l^*$. Maximal correlation (light yellow in Fig. 1) corresponds to an homogeneous deformation $\bar{\epsilon} \lesssim 10^{-7}$, and vanishing correlation (black in Fig. 1) corresponds to $\bar{\epsilon} \gtrsim 10^{-5}$. For heterogeneous deformations localized at the scale of l^*, treating the deformation as homogeneous leads in practice to a correct estimate of the magnitude of the deformation.

From isolated localized events to shear band formation.—We first monitor the mechanical behavior of the system when submitted to an increasing shear stress, a typical response being displayed in the Supplemental Material movie1.avi [31]. Figure 1(b) shows the stress as a function of time at a constant motor rotation velocity. The stress increases linearly with the rotation as expected for an elastic material connected to a torsion spring. As the rotation is increased, small stress drops are first observed (precursor events) at a stress σ_r to up to the maximal yield-stress value σ_Y. For a given confining pressure, typical reproducibility on stress values σ_r and σ_Y is 10%. Then,

the system reaches after a few rupture events a regular stick-slip motion. This is to be expected for a soft torsion spring, driven at constant rotation rate and coupled with a material displaying both static and dynamic friction thresholds. Here we are interested only in the first part of the dynamics, up to σ_Y. The onset of precursor events was described by Nguyen *et al.* [32], and a similar phenomenology was also reported in many other amorphous glassy materials [9]. The DWS imaging of the top surface is shown in Fig. 1(c). In the quasielastic part of the loading curves, the intensity correlation stays at $g_I \simeq 0.99$ except over small areas [31], the hot spots, where a significant localized correlation drop down to $g_I \lesssim 0.95$ is observed [see Fig. 1(c)]. The appearance of hot spots persists at large deformations all over the ramp test up to the steady stick-slip regime.

The extent of these spots is typically $\xi \approx 3$ mm [Fig. 2(a)] with a duration $\tau < 1$ s [Fig. 2(b)]. The corresponding local deformation amplitude may be estimated from the decorrelation of the backscattered light [29,30]: $\epsilon \simeq 5 \times 10^{-6}$. Figure 1(d) shows successive maps corresponding to the first stress drop (see also the Supplemental Material movie1.avi [31]). As the deformation is increased, more and more hot spots appear ($t = 105$–107 s). These events aggregate in clusters ($t = 107$–109 s). Finally, a large and totally uncorrelated zone supersedes the clusters ($t = 110$ s). This large decorrelation zone is associated with the first macroscopic stress drop. Therefore, the process is two-scale: The localized events occur as precursors of the macroscopic failure inside the glassy material, when such failure is itself a precursor event of the final yield.

Creep experiment.—To link those localized plastic events to the global plastic deformation of the material, we perform now creep experiments fixing the applied shear stress and monitoring both the global plastic deformation and the spatially resolved deformation map. In Fig. 3 (blue symbols), we display an example of a global plastic deformation $\Delta\gamma(t)$ obtained at low applied shear stress $\sigma = 1200$ Pa, i.e., at a value smaller than the first precursor event $\sigma_r = 1700$ Pa. During this slow plastic deformation, the DWS imaging shows that the hot spots are still present and appear to be quite isolated at this level of applied stress. To quantify the relation between their appearance and the creep motion, the cumulated number of their occurrence $N(t)$ is computed and displayed on the same graph as $\Delta\gamma(t)$ (Fig. 3). The temporal evolutions of the two quantities are very similar. Therefore, the plastic deformation rate and the rate of appearance of localized event are proportional.

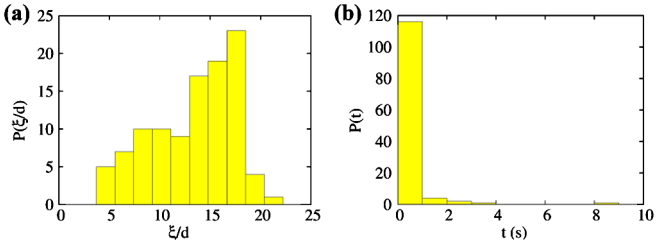

FIG. 2 (color online). Characterization of hot spots: (a) Histogram of hot-spot sizes ξ in units of bead diameter d and (b) histogram of hot-spot duration t in units of the frame cadence during the creep experiment of Fig. 3.

Soft glassy rheology.—Such creep experiments can be interpreted by using an age-dependent relaxation rate [32] reminiscent of many models derived from the soft glassy rheology. In this context, a simple viscoelastic scalar equation has been proposed [4] featuring an inverse characteristic relaxation time, the so-called fluidity $f(t)$:

$$\dot{\sigma} = G\dot{\gamma} - f(t)\sigma \tag{1}$$

with σ the applied shear stress and G a shear elastic modulus. To close the model, a constitutive relation for $f(t)$ must be provided. Many forms [4] were suggested, but, for the present case, the observed creep dynamics is consistent with the relation $\dot{f} \propto -f^2$, i.e., a relaxation time proportional to the actual age of the system (see the fit of the strain in Fig. 3). Building on the proportional relation between the rate of occurrence of hot spots and the shear rate, we propose now to go one step further and to identify $\dot{N}(t)$ with the fluidity parameter (within a proportionality constant). To test this proposition, we perform a series of creep experiments at constant applied shear stresses σ for stress values below σ_r. Figure 4 displays the relation between the cumulated number of events $N(t)$ and the total plastic strain $\Delta\gamma(t)$, at confining pressure $P_{\text{top}} = 0$ Pa (free surface). The relation is roughly linear, with slopes decreasing with the amplitude of the applied stress. By using our hypothesis of proportionality between the

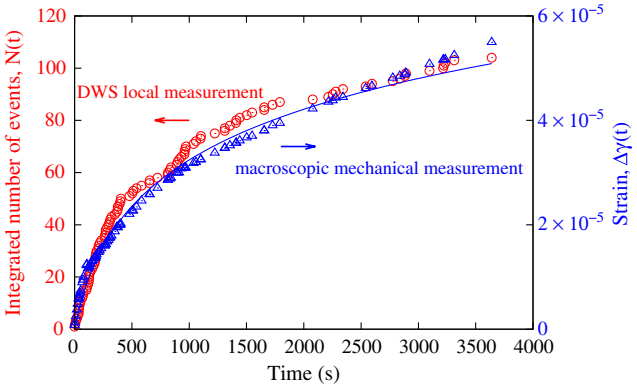

FIG. 3 (color online). Blue symbols (right axis): Strain as a function of time in a creep experiment at applied shear $\sigma = 1200$ Pa and confining pressure $P_{\text{top}} = 830$ Pa. The origin of times is defined as the moment of application of the constant stress, after a linear stress ramp lasting about 100 s. Solid blue line: Fit by a logarithmic creep law [32] $\Delta\gamma(t) = \dot{\gamma}_0 \ln(1 + Ct)/C$ with $C = 0.007$ s^{-1}. Red (left axis): Integrated number of events.

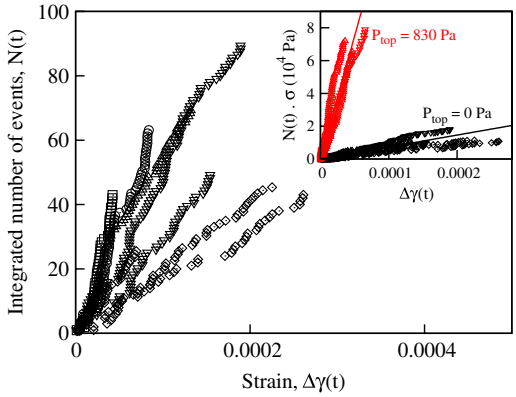

FIG. 4 (color online). Integrated number of events in a free surface experiment (confining pressure $P_{\text{top}} = 0$ Pa) for different applied shear stress: 50 (□), 100 (○), 150 (△), 200 (▽), and 250 Pa (◇). Inset: Integrated number of events multiplied by the apply shear stress for two different confining pressures, P_{top}. In black, $P_{\text{top}} = 0$ Pa: data from the main graph. In red, $P_{\text{top}} = 830$ Pa, applied shear stresses: 400, 800, 1200, and 1600 Pa.

fluidity parameter and the hot-spot rate of occurrence, integration of Eq. (1) at constant stress gives

$$G\Delta\gamma(t) = \sigma \int_0^t f(t')dt' \propto \sigma N(t). \tag{2}$$

Following this relation, it is then possible to collapse all the curves on a master straight line when multiplying $N(t)$ by the applied shear stress σ (inset in Fig. 4). To evaluate the robustness of this relation, we varied the confining pressure: Because of Hertz elasticity, the effective shear modulus G should increase with P_{top}. Indeed, for $P_{\text{top}} = 830$ Pa, the linear relation between $N(t)\sigma$ and $\Delta\gamma(t)$ holds (see the inset in Fig. 4), showing the expected qualitative stiffening (a factor of 20 approximatively). However, from a simple account of the Hertz law, we should only expect here a factor of 2. This significant difference is possibly due when $P_{\text{top}} = 0$ Pa to the presence, near the free surface, of a strong stiffness gradient and a diverging elastic susceptibility. So far, we have established a direct relation between the rate of plastic deformation and the appearance of the hot spots. Their clustering in the vicinity of major yield events *prior* to their macroscopic appearance reinforces the idea that they play a leading role in the plasticity process. However, it is not *a priori* obvious that these are the only and sufficient modes of rupture to account for the full plastic flow dynamics. Therefore, we compare an estimation of the energy released by the hot spots to the total elastic energy dissipated in the bulk. The energy dissipation of one plastic event per unit of depth is $\sigma\epsilon\xi^2$, where σ is the local stress and $\epsilon \approx \sigma/G$ the typical plastic deformation during one event. We suppose that the "hot-spot" density is uniform in the bulk. During a creep experiment, the density of energy release through the elastic bulk relaxation processes is $\sigma\Delta\gamma(t)$. Then, the energy balance per unit depth between the sum of the localized plastic dissipation $\sigma\epsilon\xi^2 N(t)$ and the bulk elastic relaxation $S\sigma\Delta\gamma(t)$ leads to the linear relation $\sigma N(t) = K\Delta\gamma(t)$ with $K = GS/\xi^2$. Quantitatively, the relation can be tested on the experiment with confining pressure $P_{\text{top}} = 830$ Pa for which the elastic response $G = 1.6 \times 10^6$ Pa has been measured (our torque probe was not sensitive enough to access the elastic regime of the $P_{\text{top}} = 0$ Pa packing). We obtain $K \approx 10^9$ Pa, close to the value obtain in the inset in Fig. 4. Therefore, within the consistency of the model, it seems that the energy released by the hot spots comes to the right magnitude to account for the macroscopic plasticity.

Conclusion.—In this Letter, we provide a direct visualization of localized deformation events associated with the mechanical response of a granular packing under shear. The optical DWS technique captures the emergence of the so-called hot spots, observed at the top surface of the shear cell and characterized by a spatial extension of about ten grains. These events are observed independently of the top surface boundary conditions: free surface or top surface covered by a glass plate and under various confining pressures. Note, in addition, that hot spots were recently identified in a DWS side observation of an inclined granular cell [33], so they seem to be generic features of granular yield properties. In this Letter, we show that hot spots are directly correlated to global mechanical measurements such as stress drops and creep dynamics, and, though they are not a direct visualization of bulk reorganizations, our results suggest that such localized events also occur in the bulk. Under a stress ramp, we show that these events increase in density with the stress amplitude and cluster spatially as precursors of a macroscopic shear band. Under constant applied shear stress, the rate of appearance of these hot spots at the top surface is proportional to the rate of plastic deformation. Varying the applied shear and the confinement stress, we point that at first approximation—possibly corresponding to a mean-field approximate of the problem—the hot-spot dynamics is in direct relation with a parameter called fluidity defined in the context of soft glassy rheology and representing the mean rate of stress relaxation. Our study points out the interest of clarifying this relation, by characterizing the spatiotemporal coupling of the hot-spot dynamics, in particular, in the vicinity of the material yield or under sustained mechanical noise. These results provide some substantial experimental evidence backing many theoretical propositions made recently about zero temperature plasticity of amorphous solids. It focuses the debate on the importance of localized precursor events participating in the yield dynamics, a concept which can be crucial in a wide context encompassing solid disordered system, complex fluids, or even earthquake dynamics.

We acknowledge the financial support of the CNES-GDR 2799 program, the ANR projects "Jamvibe-2010"

and "STABINGRAM" No. 2010-BLAN-0927-01. E. C. thanks Bruno Andreotti for many scientific discussions; A. A. and J. C. thank Patrick Chasles for help with the image acquisition.

[1] L. Berthier and G. A. Biroli, *Statistical Mechanics Perspective on Glasses and Aging Encyclopedia of Complexity and Systems Science* (Springer, New York, 2008).
[2] P. Sollich, F. Lequeux, P. Hébraud, and M. E. Cates, Phys. Rev. Lett. **78**, 2020 (1997).
[3] P. Sollich, Phys. Rev. E **58**, 738 (1998).
[4] C. Derec, A. Ajdari, and F. Lequeux, Eur. Phys. J. E **4**, 355 (2001).
[5] J. Goyon, A. Colin, G. Ovarlez, A. Ajdari, and L. Bocquet, Nature (London) **454**, 84 (2008).
[6] R. Besseling *et al.*, Phys. Rev. Lett. **105**, 268301 (2010).
[7] A. Kabla and G. Debregeas, J. Fluid Mech. **587**, 23 (2007).
[8] A. Kabla, J. Scheibert, and G. Debregeas, J. Fluid Mech. **587**, 45 (2007).
[9] A. Tanguy, F. Leonforte, and J.-L. Barrat, Eur. Phys. J. E **20**, 355 (2006).
[10] P. Schall and M. van Hecke, Annu. Rev. Fluid Mech. **42**, 67 (2010).
[11] Thibaut Divoux, David Tamarii, Catherine Barentin, and Sébastien Manneville, Phys. Rev. Lett. **104**, 208301 (2010).
[12] D. Klaumünzer *et al.*, Phys. Rev. Lett. **107**, 185502 (2011).
[13] K. A. Dahmen, Y. Ben-Zion, and J. T. Uhl, Nature Phys. **7**, 554 (2011).
[14] A. S. Argon, Acta Metall. **27**, 47 (1979).
[15] M. L. Falk and J. S. Langer, Phys. Rev. E **57**, 7192 (1998).
[16] C. E. Maloney and A. Lemaître, Phys. Rev. E **74**, 016118 (2006).
[17] A. Lemaître and C. Caroli, Phys. Rev. Lett. **103**, 065501 (2009).
[18] E. Lerner and I. Procaccia, Phys. Rev. E **80**, 026128 (2009).
[19] S. M. Talamali, V. Petäjä, D. Vandembroucq, and S. Roux, arXiv:1005.2463.
[20] G. Picard, A. Ajdari, L. Bocquet, and F. Lequeux, Phys. Rev. E **66**, 051501 (2002).
[21] L. Bocquet, A. Colin, and A. Ajdari, Phys. Rev. Lett. **103**, 036001 (2009).
[22] J. Goyon, A. Colin, and L. Bocquet, Soft Matter **6**, 2668 (2010).
[23] G. Katgert, B. P. Tighe, M. E. Mobius, and M. van Hecke, Europhys. Lett. **90**, 54 002 (2010).
[24] A. Kabla and G. Debrégeas, Phys. Rev. Lett. **90**, 258303 (2003).
[25] P. Schall, D. A. Weitz, and F. Spaepen, Science **318**, 1895 (2007).
[26] S. Nasuno, A. Kudrolli, and J. P. Gollub, Phys. Rev. Lett. **79**, 949 (1997).
[27] S. Nasuno, A. Kudrolli, A. Bak, and J. P. Gollub, Phys. Rev. E **58**, 2161 (1998).
[28] M. Erpelding, A. Amon, and J. Crassous, Phys. Rev. E **78**, 046104 (2008).
[29] J. Crassous, Eur. Phys. J. E **23**, 145 (2007).
[30] M. Erpelding, A. Amon, and J. Crassous, Europhys. Lett. **91**, 18 002 (2010).
[31] See Supplemental Material at http://link.aps.org/supplemental/10.1103/PhysRevLett.108.135502 for movies. movie1.avi is the visualization of the imposed deformation experiment shown in Fig. 1 from $t = 0$ to 700 s, confining pressure $P_{\text{top}} = 80$ Pa. movie2. avi shows a typical creep experiment at constant stress: The stress is first increased and then kept constant. Confining pressure, $P_{\text{top}} = 0$ Pa; shear stress, $\sigma = 100$ Pa. Analysis of creep starts after the initial stress ramp.
[32] V. B. Nguyen, T. Darnige, A. Bruand, and E. Clément, Phys. Rev. Lett. **107**, 138303 (2011).
[33] A. Amon, R. Bertoni, and J. Crassous (to be published).